



ELSEVIER

Optical Materials 17 (2001) 179–183



www.elsevier.nl/locate/optmat

Type-II antimonide quantum wells for mid-infrared lasers

M.J. Yang ^{a,*}, J.R. Meyer ^a, W.W. Bewley ^a, C.L. Felix ^a, I. Vurgaftman ^a,
W. Barvosa-Carter ^b, L.J. Whitman ^a, R.E. Bartolo ^a, D.W. Stokes ^a,
H. Lee ^c, R.U. Martinelli ^c

^a Naval Research Laboratory, 4555 Overlook Ave. S.W. Washington, DC 20375, USA

^b HRL Laboratories, Malibu, CA 90256, USA

^c Sarnoff Corporation, CN 5300, Princeton, NJ 08543-5300, USA

Abstract

This paper discusses some of the key MBE growth issues for type-II Sb-based lasers, and present a summary of our recent progress towards the realization of high-power, high-beam-quality, mid-infrared (IR) lasers based on the “W” configuration of the active region. An optical pumping injection cavity (OPIC) approach has been adopted to improve the external power conversion efficiency. In addition, the first mid-IR angled-grating distributed feedback (α -DFB) lasers producing near-diffraction-limited output is discussed. © 2001 Elsevier Science B.V. All rights reserved.

Keywords: MBE; Infrared lasers; Antimonide quantum wells

1. Introduction

The demand for mid-infrared (IR) (3–5 μm) lasers is on the horizon in various areas. In some cases, high output power is preferred. On the other hand, to identify the fingerprints of trace chemical species with high-resolution spectroscopy, a cw output power of $>200 \mu\text{W}$ is sufficient. In this case, it is necessary to have a single-mode output and a means of tuning the wavelength. To commercialize such an instrument for the chemical sensing application, the laser needs to operate at ambient temperature or with thermoelectric cooling to reduce cost. In addition, cw operation provides improved stability and reliability.

For many years, the only mid-IR laser (3–30 μm) commercially available was the lead salt diode [1]. That material system suffers from low thermoconductivity and susceptibility to damage, which limit its output power and operating temperature. Type-I antimonide-based lasers [2–4], e.g., using InAsSb quantum wells, have performed well at 77 K in the range of $\lambda = 3\text{--}4 \mu\text{m}$. However, the shallow carrier confinement and high Auger recombination rates become problematic for high-temperature operation due to prohibitively high-thresholds. A third approach, the quantum cascade laser (QCL) [5,6], has demonstrated cw lasing at cryogenic temperatures for 3.4–17 μm . Due to the nature of the conduction band offset in InGaAs-based QCLs, it is quite difficult for lasers at $\lambda < 4.5 \mu\text{m}$ to have reasonable output power. In addition, the relatively high-threshold current resulting from the high phonon scattering rate makes it quite challenging to develop QCLs

* Corresponding author. Tel.: +1-202-404-4516; fax: +1-202-767-1165.

E-mail address: yang@bloch.nrl.navy.mil (M.J. Yang).

capable of cw operation up to TE-cooled or ambient temperatures.

In this paper, we report an investigation of another emerging IR system, namely type-II antimonide quantum wells [7–9]. In particular, we consider type-II “W” lasers, which are named for the shape of the conduction-band profile in its four-constituent active region, e.g., InAs/InGaSb/InAs/AlSb. This system has the record for the highest pulsed output power at ambient temperature in 3–5 μm . It has also demonstrated cw operation at $\lambda \leq 4 \mu\text{m}$ and $T > 240 \text{ K}$, which is achievable by thermoelectric cooling. Not only can the type-II lasers have low thresholds due to the suppression of Auger recombination, but the W structure also benefits from the combination of a two-dimensional density of states for both electrons and holes, strong wavefunction overlap for high-gain, and high-conduction and valence band offsets for efficient electrical confinement.

2. Molecular beam epitaxy growth

Recently, we reported the importance of the molecular beam epitaxy (MBE) growth temperature for InAs/InGaSb/AlSb IR laser structures [10]. We have successfully applied IR transmission thermometry to provide an accurate temperature measurement of GaSb substrates and a GaSb surface reconstruction transition has been established as a laboratory-independent temperature standard [11]. Several critical growth parameters that affect the properties of type-II IR laser structures have also been investigated.

It was found that the range of optimum growth temperatures is relatively narrow, at most from 400°C to 450°C. A higher growth temperature results in the formation of clusters in InGaSb quaternary layers. Fig. 1 shows the cross-sectional STM images of 12-monolayer InGaSb sandwiched by InAs for two samples grown at 435°C and 500°C. Note that only every other (001) growth layer is exposed on a {110} cleave. The clustering observed in the high- T sample accounts for the lower photoluminescence (PL) intensity and the broadened PL linewidth. We also found that laser

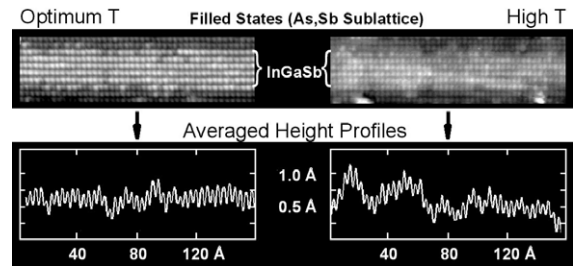


Fig. 1. Cross-sectional STM images and the averaged height profiles of InGaSb layers in two samples grown at different temperatures.

structures with InSb-like interfacial bonds and grown using a cracked Sb source have better PL efficiency. To assure the formation of InSb-like interfacial bonds at every interface, migration enhanced epitaxy was employed.

Fig. 2 displays an STM image of a four-constituent W structure grown under optimized conditions. The group V to III flux ratio is maintained at ~ 2 in all layers. Although this sample displayed excellent PL characteristics, several imperfections revealed in the image need further improvement. For example, contamination of both Sb in the InAs layer and In in the AlSb layer has been observed. In addition, although Sb-like bonds are intended, the STM image still reveals an alternating Sb- or As-bonding at the InAs/AlSb interfaces. The sensitivity of the bond type to growth order probably depends on a complicated thermodynamic balance.

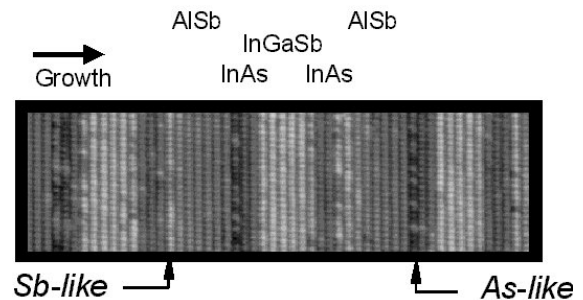


Fig. 2. Cross-sectional STM image of a W-structure grown at 435°C with cracked antimony source and an intended Sb-like interfacial bonds by migration enhanced epitaxy.

3. Optical pumping injection cavity (OPIC) lasers

The open boxes of Fig. 3 are the maximum cw operating temperatures for optically pumped ($\lambda_{\text{pump}} = 1.06 \mu\text{m}$ Nd:YAG) W lasers employing diamond pressure bond (DPB) heat sinking, which are higher than any other semiconductor lasers at wavelengths between $3.0 \mu\text{m}$ (290 K) and $6.1 \mu\text{m}$ (210 K) [12]. For 77 K operation, DPB-mounted optically pumped W lasers have also displayed higher output powers than any other mid-IR semiconductor lasers. The maximum cw power for a device emitting at $\lambda = 3.2 \mu\text{m}$ was 0.54 W, while the maximum quasi-cw (25% duty cycle) power was 0.76 W. However, the cw output fell to 40 mW at 180 K, due to large internal losses caused by strong free carrier absorption.

In order to continue increasing the high-temperature performance of these lasers, improvements in the thresholds, conversion efficiency, and internal loss will be needed. To achieve this, we would like to combine a high-pump absorptance with a long pump wavelength and an active layer with few quantum wells. We have made encouraging progress toward that objective using the OPIC approach [13], in which the active region is enclosed in an etalon cavity whose resonance is tuned to the pump wavelength. Experiments on MBE-grown structures containing semiconductor Bragg mirrors above and below the active QWs

confirm that the multiple passes of the pump result in three significant advantages. First, the pump absorptance can be high at long wavelength, e.g., $\lambda_{\text{pump}} \approx 2 \mu\text{m}$, despite a weak absorption of each single pass. Second, the lasing threshold is reduced, and third, the internal loss due to free carrier absorption is also reduced.

Cavities for the fabricated OPIC structures were formed by growing GaSb/AlAsSb distributed Bragg reflectors (DBRs) above and below the W active region. At the mid-IR lasing wavelength those stacks simply function as low-index optical cladding layers, and the laser operates conventionally as an edge emitter. Even with only 10 QWs present (compared to 50–80 in most of the earlier non-OPIC W devices), absorptances of 57–71% were measured for pumping by a $2.098 \mu\text{m}$ Q-switched Ho:YAG laser. Since the wavelength of the pump beam was fixed, tuning to the cavity resonance condition at each temperature was accomplished by varying the angle of incidence on the sample.

The differential power efficiencies for two OPIC structures (each containing 10 QWs) and a similar-wavelength W laser without a pump cavity (80 QWs) are plotted in Fig. 4. For W-OPIC-2, the efficiency at 100 K is seen to be 11.4% per facet, which compares with 8.3% for W-OPIC-1 and 1.8% for the conventional W laser. Furthermore, the efficiency for W-OPIC-2 degrades quite slowly

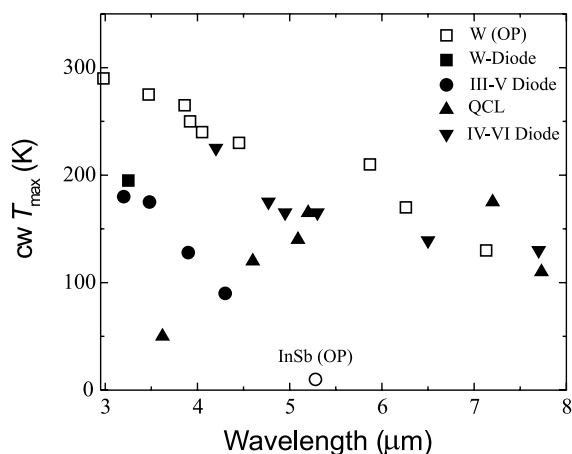


Fig. 3. Maximum cw operating temperatures vs. wavelength in the 3–8 μm range for various types of infrared lasers.

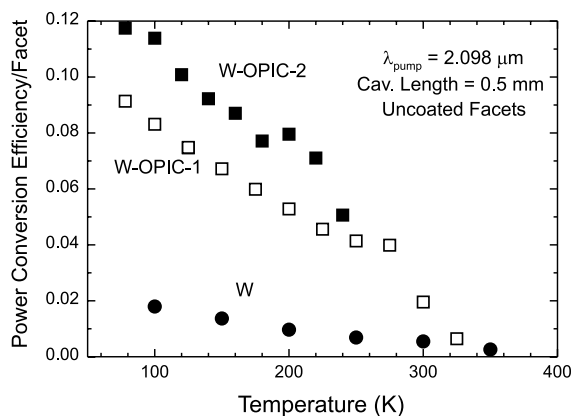


Fig. 4. Pulsed incident differential power efficiency vs. temperature for two OPIC lasers and a conventional W laser. In all cases, pumping was by 107 ns pulses from a Ho:YAG laser.

with increasing temperature. For example, it still exceeds 7% per facet at 220 K and in W-OPIC-1 it exceeds 4% at 275 K.

The high external conversion efficiencies are due to the strong absorbance of the pump beam that results from its multiple passes through the active region, and the low internal losses. The internal loss for W-OPIC-2 was found to be 5.5 cm^{-1} at 78 K and 20 cm^{-1} at 240 K, the latter of which is more than a factor of 3 lower than any previous result for an interband mid-IR laser. In addition, the thresholds for both OPIC devices were significantly suppressed by a factor of 6 at 80 K to 4 at 300 K in comparison with the conventional W laser. Due to slightly higher absorbance of the bump beam (71% vs. 57%) and slightly longer Shockley–Read lifetime, the threshold in W-OPIC-2 is lower than that in W-OPIC-1 at low T , e.g., 70 W cm^{-2} at 78 K. In view of the low-thresholds and high-efficiencies, it appears likely that the W-OPIC approach will ultimately lead to high cw output powers at thermoelectric-cooler temperatures.

4. Mid-infrared angled-grating distributed feedback (α -DFB) lasers

Some sensing applications call for good beam quality in addition to the spectral purity of single-mode output. The angled-grating DFB laser, or α -DFB, has been particularly successful at combining those attributes in the visible and near-IR [14]. A diffraction grating is etched into the laser cavity at an angle with respect to the facets. The beating of two waves having mode profiles concentrated on opposite sides of the stripe causes the net optical intensity to zig-zag from side-to-side as the beam propagates along the angled cavity. Upon reaching the facet, only those components of the optical wave that impinge nearly at normal incidence have appreciable feedback, which leads to very low angular divergence of the output beam. Spectral selectivity can also occur, due to the wavelength dependence of the diffraction grating.

At wavelengths in the 0.66–1.06 μm range, α -DFB lasers have displayed near-diffraction-limited beam qualities combined with high-cw output powers and single-mode emission with

excellent sidemode suppression. As a first step toward attaining similar properties in the mid-IR, we recently fabricated and tested optically pumped α -DFB W lasers [15]. The MBE-grown structure consisted of a 2.5- μm -thick AlSbAs lower optical cladding layer, the W active region, a thin AlSbAs hole-blocking layer, and a separate-confinement region consisting mostly of GaSb. A combination of dry and wet etching was used to pattern the $\sim 800 \text{ \AA}$ -deep grating into the top GaSb with a 1.9 μm period and 16° angle relative to the facet normal. The laser bar with a cavity length of 1.4 mm contained both a grating region and an unpatterned region, so that the α -DFB and Fabry–Perot performances could be compared directly under identical pulsed optical pumping conditions (at 2.098 μm) using adjacent wafer material.

The spectral narrowing for these devices emitting at $\lambda \approx 3.4 \mu\text{m}$ was only a factor of 2. Preliminary modeling suggests that the lack of single-mode emission may be related to the relatively large background internal losses. Nonetheless, far-field scans confirmed that the α -DFB output was nearly diffraction-limited. Fig. 5 compares lateral far-field profiles for the α -DFB and Fabry–Perot lasers. The full-width at half-maximum (FWHM) divergence angle for the roughly gaussian α -DFB output was only 1.4° ,

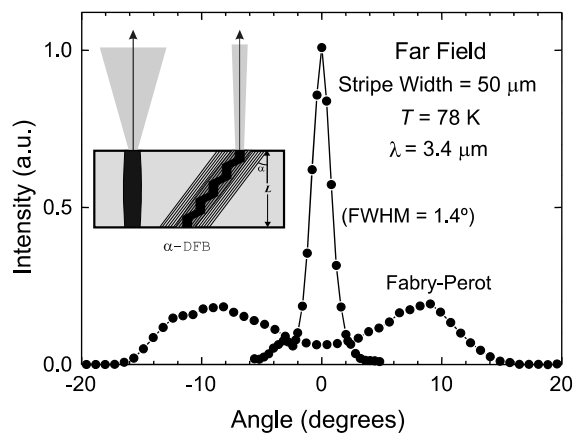


Fig. 5. Pulsed far-field angular profiles for an optically pumped α -DFB laser and a Fabry–Perot laser from an unpatterned portion of the same bar at 78 K. The inset shows the schematic top views of these two types of lasers.

compared to a divergence of 25° for the double-lobed Fabry–Perot profile. Along the fast axis, the two lasers had nearly identical single-lobed profiles with FWHM divergences of 24° . The slope efficiency of the α -DFB was 64% of that for the Fabry–Perot device, and the threshold was 15% lower. Thus the remarkable improvement of the beam quality comes at a relatively modest cost in net output power. This makes the potential for high-brightness mid-IR sources quite promising.

5. Conclusions

The MBE growth for antimonide-based material has been studied much less than other III–V compounds such as GaAs and InP. In addition, due to the lack of detailed understanding of the fundamental properties, e.g., band structure of individual constituent layer for W lasers, and band alignment for different alloys under different degrees of strain, the design of type-II lasers is still far from optimum. Despite these difficulties, the preliminary results for a variety of type-II lasers have demonstrated high-output-power capability, and outperformed the other competing systems in the range of 3–5 μm . Since the carrier absorption becomes stronger as the wavelength gets longer, we need intelligent device design to minimize the internal loss for $\lambda > 5 \mu\text{m}$. With the flexibility of band structure engineering in the type-II antimonide system, it is foreseeable that the rapid advances of the laser performance will continue.

Acknowledgements

The work at NRL was supported by the Office of Naval Research and the Air Force Research Laboratory. The work at Sarnoff was supported by an ONR phase-II SBIR.

References

- [1] M. Tacke, *Infrared Phys. Technol.* 36 (1994) 447.
- [2] H.K. Choi, et al., *Appl. Phys. Lett.* 65 (1994) 2251.
- [3] H.K. Choi, et al., *Appl. Phys. Lett.* 67 (1995) 332.
- [4] H.K. Choi, et al., *Appl. Phys. Lett.* 68 (1996) 2936.
- [5] F. Capasso, et al., *IEEE J. Sel. Topic in Quant. Elec.* 5 (1999) 792.
- [6] F. Capasso, et al., *Phys. World* 12 (1999) 27.
- [7] H.Q. Le, C.H. Lin, S.J. Murry, R.Q. Yang, S.S. Pei, *IEEE J. Quant. Elec.* 34 (1998) 1016.
- [8] R.Q. Yang, J.D. Bruno, J.L. Bradshaw, J.T. Pham, D.E. Wortman, *Physica E* 7 (2000) 69.
- [9] I. Vurgaftman, C.L. Felix, W.W. Bewley, D.W. Stokes, R.E. Bartolo, J.R. Meyer, *Phil. Trans. Roy. Soc. London A*, in press.
- [10] M.J. Yang, W.J. Moore, B.R. Bennett, B.V. Shanabrook, J.O. Cross, I. Vurgaftman, W.W. Bewley, C.L. Felix, J.R. Meyer, *J. Appl. Phys.* 86 (1999) 1796.
- [11] M.J. Yang, W.J. Moore, C.H. Yang, R.A. Wilson, B.R. Bennett, B.V. Shanabrook, *J. Appl. Phys.* 85 (1999) 6632.
- [12] W.W. Bewley, C.L. Felix, I. Vurgaftman, D.W. Stokes, E.H. Aifer, L.J. Olafsen, J.R. Meyer, M.J. Yang, B.V. Shanabrook, H. Lee, R.U. Martinelli, A.R. Sugg, *Appl. Phys. Lett.* 74 (1999) 1075.
- [13] C.L. Felix, W.W. Bewley, I. Vurgaftman, L.J. Olafsen, D.W. Stokes, J.R. Meyer, M.J. Yang, *Appl. Phys. Lett.* 75 (1999) 2876.
- [14] B. Pezeshki, M. Hagberg, M. Xelinske, S.D. DeMars, E. Kolev, R.J. Lang, *IEEE Phot. Tech. Lett.* 11 (1999) 791.
- [15] R.E. Bartolo, W.W. Bewley, I. Vurgaftman, C.L. Felix, J.R. Meyer, M.J. Yang, *Appl. Phys. Lett.* 76 (2000).